



HAL
open science

Interaction between deformation and sedimentation in a multidecollement thrust zone: Analogue modelling and application to the Sub-Andean thrust belt of Bolivia

Lena Driehaus, Thierry Nalpas, Jean-François Ballard

► **To cite this version:**

Lena Driehaus, Thierry Nalpas, Jean-François Ballard. Interaction between deformation and sedimentation in a multidecollement thrust zone: Analogue modelling and application to the Sub-Andean thrust belt of Bolivia. *Journal of Structural Geology*, 2014, 65, pp.59-68. 10.1016/j.jsg.2014.04.003 . insu-00993481

HAL Id: insu-00993481

<https://insu.hal.science/insu-00993481>

Submitted on 20 May 2014

HAL is a multi-disciplinary open access archive for the deposit and dissemination of scientific research documents, whether they are published or not. The documents may come from teaching and research institutions in France or abroad, or from public or private research centers.

L'archive ouverte pluridisciplinaire **HAL**, est destinée au dépôt et à la diffusion de documents scientifiques de niveau recherche, publiés ou non, émanant des établissements d'enseignement et de recherche français ou étrangers, des laboratoires publics ou privés.

1 **Interaction between deformation and sedimentation in a multidecollement thrust zone:**
2 **analogue modelling and application to the Sub-Andean thrust belt of Bolivia**

3 Lena DRIEHAUS ^{a,b}, Thierry NALPAS ^{a,*}, Jean-François BALLARD ^c

4
5 a Géosciences Rennes, Université de Rennes 1, UMR 6118 du CNRS, Campus de Beaulieu, 35042 Rennes cedex,
6 France

7 b Departament de Geodinàmica i Geofísica, Facultat de Geologia, Universitat de Barcelona (UB) C/ Martí i Franquès
8 s/n, 08028-Barcelona, Spain.

9 c Total EP, CSTJF, Avenue Larribau, 64018 Pau Cédex, France

10 * Corresponding author. Tel.: +33 223235675; fax: +33 223236100.

11 E-mail address: thierry.nalpas@univ-rennes1.fr (T. Nalpas).

12
13 Keywords: Compressive system; Decollement; Synkinematic sedimentation; Experiment; Incahuasi

14
15
16 **ABSTRACT**

17 Fold and thrust belts are influenced by the presence of decollement levels, as well as the amount of
18 shortening and synkinematic sedimentation. These parameters are studied at the scale of a thrust
19 belt using a field approach, combined with analogue and numerical modelling. In this study, we use
20 analogue modelling to test the evolution of a single structure during sedimentation in a domain
21 containing three prekinematic decollement levels. The development of this structure in the analogue
22 experiments shows that the expression of the deformation is strongly dependent on sedimentation
23 rate: (i) the structure propagates forward in an overall asymmetric shape if the sedimentation rate is
24 slower than the uplift velocity, or (ii) the structure grows vertically and its vergence changes at the
25 surface if the sedimentation rate is similar to the uplift velocity, or (iii) the structure grows

26 vertically with a double vergence at the surface and at depth if the sedimentation rate is higher than
27 the uplift velocity. The results of the experiments are compared with structures in the Subandean
28 thrust belt to aid the interpretation of poor seismic data.

29

30 **1. Introduction**

31 The deformation observed in compressive systems such as fold and thrust belts is influenced by the
32 presence of decollement levels (e.g. Dunn et al., 1995; Labaume and Moretti, 2001; Sepehr et al.,
33 2006; Verges et al., 2011), which exhibit low basal friction related to lithology (marl, shale, coal
34 and evaporite) and/or overpressure conditions (e.g. Cobbold and Rodrigues, 2007; Cobbold et al.,
35 2009). These systems have been investigated in previous analogue studies that show the importance
36 of the basal angle of the wedge and the shortening rate (e.g. Smit et al., 2003), as well as the
37 presence of decollement levels in controlling coupling/decoupling processes (e.g. Couzens-Schultz
38 et al., 2003; Massoli et al., 2006) and synkinematic sedimentation (Leturmy et al., 2000). The
39 relationship between sedimentation and thrust geometry at the scale of a single structure has been
40 studied using analogue modelling with one prekinematic ductile layer (Nalpas et al., 1999; Casas et
41 al., 2001; Barrier et al., 2002; Nalpas et al.; 2003; Gestain et al., 2004; Barrier et al., 2013).
42 However, only one study has been carried out at the scale of a single structure with two
43 prekinematic ductile layers (Pichot and Nalpas, 2009), so there is a continuing debate about the
44 vergence of the thrusts as well as the evolution of deformation at depth and at the surface in relation
45 to mass transfer.

46 This study makes use of analogue modelling to investigate the formation and evolution of a
47 compressive structure with a mechanical stratigraphy comprising three prekinematic decollement
48 levels (ductile layers) according to (i) the amount of shortening and (ii) the synkinematic rate of
49 mass transfer. The results of this experimental approach are then compared with a field example
50 (the Subandean thrust-belt).

51 **2. Experimental procedure**

52 In this study, we apply the classical techniques used for brittle-ductile analogue modelling
53 experiments developed by the Experimental Tectonics Laboratory of Géosciences Rennes
54 (Université de Rennes 1, France). These techniques have been described in previous studies dealing

55 with the use of a velocity discontinuity (VD; e.g. Malavieille, 1984; Balé, 1986; Ballard et al., 1987;
56 Allemand et al., 1989), the use of silicone and sand (Faugère and Brun, 1984), and also various
57 scaling issues (Davy and Cobbold, 1991; Weijermars et al., 1993). Brittle layers (pre- and
58 synkinematic) are represented by dry Fontainebleau quartz sand, with an internal friction angle of
59 30-35° (Krantz, 1991) and a density (ρ) of approximately 1,500 kg/m³. The weak ductile layers (e.g.
60 salt, clay) are represented by i) pink silicone putty 70 009 (Rhône Poulenc, France) with a viscosity
61 (μ) of around 10⁴ Pa·s at 20°C and a density (ρ) close to 1,400 kg/m³, and ii) transparent silicone
62 putty SGM 36 (Dow Corning, USA) with a viscosity (μ) of around 10⁴ Pa·s at 20°C and a density
63 (ρ) close to 1,000 kg/m³.

64 Silicone putty is commonly used to model salt, but it has also been used to model overpressured
65 shales (e. g. Cohen and McClay, 1996; Wu and McClay, 2011). To take into account overpressures
66 and pore fluids in decollement levels such as shales, physical modelling techniques have been
67 developed using compressed air injected into beeswax microspheres (e.g. Cobbold and Castro,
68 1999; Cobbold et al., 2001; Mourgues and Cobbold, 2003; Zanella et al., 2014). The
69 implementation of these techniques is complicated and remains impractical for experiments with
70 three decollement levels, explaining why such an approach is not adopted here.

71 The experimental apparatus consists of a fixed wall screwed to a rigid and fixed basal plate, over
72 which another wall fixed to a thin mobile basal plate is pushed at a constant rate (Fig. 1a). The two
73 other sides are free and supported by sand to ensure uniform stresses. The displacement of the basal
74 mobile plate induces a velocity discontinuity (VD) at its border, which localizes the deformation at
75 the base of the model, (cf. Malavieille, 1984; Balé, 1986; Ballard, 1989). In our experiments, we use
76 a VD to simulate only one structure, with the VD representing the zone localizing the deformation
77 at the base of the model. The VD may represent either a basement fault, (e.g. Richard et al., 1991)
78 or, in an imbricate thrust system, the tip line of a basal decollement (Boyer and Elliot, 1982; Casas
79 et al., 2001). The experiment is set up in a 100 x 60 cm sandbox, wide enough to allow the model to
80 be cut into several vertical slices after each phase of deformation without border effects (see below).

81 To facilitate comparisons with natural examples such as the Bolivian Subandean fold and thrust
82 belt, where several decollement levels are present, we set up experiments composed of a four-layer
83 brittle-ductile system. The prekinematic pile consists of layers including, from bottom to top: 1 cm
84 of purple silicone (lower decollement level); 1.2 cm of black and white sand; 0.8 cm of transparent
85 silicone (middle decollement level); and 3 cm of black and white sand. The layer of black and white

86 sand is composed of two 1.5 cm layers separated by a thin layer (0.3 cm) of silicone to facilitate
87 flexural slip (Fig. 1a). The synkinematic pile is composed of blue and white sand layers of different
88 thicknesses. To simulate synkinematic mass transfer, both sedimentation and erosion are simulated.
89 Sedimentation is simulated using fresh sand (blue and white) that is continuously sprinkled
90 manually onto the model during the shortening (e.g. Cobbold et al., 1993; Baby et al., 1995; Storti
91 and McClay, 1995; Barrier et al., 2002). Erosion is simulated by removing sand with a vacuum
92 cleaner. To define the amount of sedimentation, we use the dimensionless parameter $R = V_s/V_u$,
93 where R is the ratio between the rate of the sedimentation (V_s) and the velocity of uplift of the
94 structure (V_u) (see Barrier et al., 2002; Pichot and Nalpas, 2009). To define the amount of erosion,
95 we use a dimensionless parameter $E = V_e/V_u$, where E is the ratio between the velocity of the
96 erosion (V_e) and the velocity of uplift of the structure (V_u). The switchover between erosion and
97 sedimentation corresponds to a base level in the stratigraphic sense (Posamentier et al., 1988;
98 Posamentier and Vail, 1988), which implies that the system is being eroded above the base level,
99 with transit occurring along this level and sedimentation below. Different sedimentation modes are
100 chosen to represent the range of possible sedimentation rates within natural basins (Fig. 1b). In the
101 first series of experiments, models are performed without sedimentation ($R = 0$), the second series
102 with sedimentation and erosion ($R = 1/2$ and $E = 1/4$), the third series with sedimentation alone ($R =$
103 1) and the fourth series with a high sedimentation/uplift ratio ($R = 2$). The variations of mass
104 transfer between our experiments are comparable to different geographic positions in the Bolivian
105 Subandean fold and thrust belt, ranging from the western zone with erosion, through the central
106 foredeep with a high sedimentation rate to the eastern zone with a low sedimentation rate.

107 Table 1 presents the geometric and dynamic scaling of the models. The scale ratios for dimensions
108 and stress between the models and nature are of the same order of magnitude (10^{-5}), and the
109 shortening rate is imposed by the scaling laws. A velocity of 1 cm/h is used for displacement of the
110 piston, mobile basal plate and wall, along with the associated velocity discontinuity (VD).
111 Photographs of the model surface are taken at regular time intervals (every 15 min) to observe the
112 development of the structure. Sand layers are made up of various colours; black and white for the
113 prekinematic layers, and blue and white for the synkinematic layers (the colour of the sand does not
114 modify its behaviour). After deformation, the internal structures and their time-evolution are
115 observed in a series of cross-sections cut parallel to the compression direction and perpendicular to
116 the VD. The experiments are conducted in three steps of shortening: i) compression of 5 cm; ii)
117 compression of 7.5 cm; and iii) compression of 10 cm. All the cross-sections extracted after each

118 step are taken at a distance of at least 5 cm from the lateral border of the model, in order to avoid
119 boundary effects. The deformation is not affected by stopping between steps. This is verified by an
120 experiment in which 10 cm of shortening in one step yields the same amount of deformation as the
121 experiment performed in 3 shortening steps. Although a total of twenty experiments were
122 performed to test the reproducibility (denoted Bode 1 to Bode 20), only the results of four
123 experiments are presented here.

124 To simplify the description of the silicone/sand pile of the model, we use the following terminology
125 (Fig. 2). From bottom to top, the prekinematic layers are called: lower silicone layer; lower sand
126 layer; middle silicone layer; middle sand layer; upper silicone layer; upper sand layer. The layers
127 added during the experiment are termed synkinematic sand layers. The thrusts are named according
128 to the sand layers affected and their geometry in relation to the VD inducing shear displacement
129 (Ballard, 1989). For example, a synthetic thrust occurs when the hanging wall moves in a direction
130 opposite to the movement of the mobile plate, and an antithetic thrust is characterized by the
131 hanging wall moving in the same direction as the mobile plate. Therefore, as shown in Figure 2, the
132 thrusts are referred to as follows, from bottom to top: lower synthetic thrust; middle antithetic
133 thrust; upper synthetic thrust. The faults are colour coded to highlight the movement of the faults
134 for each step of deformation (Fig. 3). The forward or backward propagation of the deformation is
135 defined with respect to the previous structure considered (Fig. 2).

136 **3. Results of analogue modelling experiments**

137 *3.1. Shortening without sedimentation, $R = 0$ (Fig. 3a)*

138 The main feature observed in this experiment is the synthetic vergence of all thrusts, associated with
139 a forward propagation of the deformation.

140 More precisely:

141 - After 5 cm of shortening (Fig. 3a1), the lower and middle sand layers are affected by synthetic
142 thrusts generating penetration of the lower and middle sand layers into the middle and upper
143 silicone layers, respectively. The upper sand layer is affected by a synthetic thrust with a very
144 shallow dip.

145 - After 7.5 cm of shortening (Fig. 3a2), the anticline in the lower sand layer is amplified and
146 associated with an accumulation of silicone forming a ridge in the lower silicone layer near the VD.
147 The lower and middle synthetic thrusts grow in amplitude and are rotated anticlockwise. The upper
148 synthetic thrust is still active, and a pop-up structure develops in front of the thrust (in yellow in
149 Fig. 3a2).

150 - After 10 cm of shortening (Fig. 3a3), the lower and middle synthetic thrusts have undergone
151 anticlockwise rotation and become no longer active. In addition, a new lower synthetic thrust
152 develops (in yellow in Fig. 3a3). The upper synthetic thrust and the associated pop-up structure are
153 still active. The layers are affected by an amplification of the folding.

154 3.2. Shortening with synkinematic sedimentation and erosion, $R = 1/2$, $E = 1/4$ (Fig. 3b)

155 The main feature of this experiment is the change in vergence of the middle and upper antithetic
156 thrusts after 10 cm of shortening.

157 More precisely:

158 - After 5 cm of shortening (Fig. 3b1), the lower sand layer is affected by a synthetic thrust of flat
159 geometry that penetrates the middle silicone layer. The middle and upper sand layers are affected by
160 an antithetic thrust. Firstly, the middle antithetic thrust penetrates slightly into the upper silicone
161 layer, and then, while showing a steeper dip, it connects up with the upper antithetic thrust. The
162 upper sand layer is slightly eroded on the crest of the ramp anticline. The synkinematic layers show
163 onlap geometry on the hanging wall of the upper thrust, and toplap geometry below the base of the
164 thrust in the footwall.

165 - After 7.5 cm of shortening (Fig. 3b2), the deformation is similar to that observed for 5 cm of
166 shortening with the same synthetic and antithetic thrusts. The lower synthetic thrust shows a large
167 penetration into the middle silicone layer. An amplification of the the middle and upper antithetic
168 thrusts induces more uplift and erosion on the crest of the ramp anticline in the upper sand layer.
169 The synkinematic layers show the same overall geometry with increasing deformation.

170 - After 10 cm of shortening (Fig. 3b3), a change in the vergence of the deformation is observed. The
171 lower synthetic thrust penetrates deeply into the middle silicone layer, while an incipient lower
172 antithetic thrust is developed (in yellow in Fig. 3b3). The lower synthetic thrust is deformed, in

173 relation to a thickening of the lower silicone layer near the VD. New middle and upper synthetic
174 thrusts cut the previous middle and upper antithetic thrusts. The previous middle and upper
175 antithetic thrusts are slightly rotated clockwise and displaced passively on the hanging wall of the
176 newly formed middle and upper synthetic thrusts. The synkinematic layers deposited during the
177 growth of these synthetic thrusts show onlap geometry on their hanging wall, thus sealing the
178 previous antithetic thrust. These layers also show toplap geometry below the base of the synthetic
179 thrust in the footwall.

180 3.3. Shortening with synkinematic sedimentation, $R = 1$ (Fig. 3c)

181 The main feature of this experiment is that all the sand layers are affected by thrusts of opposite
182 vergence developing a typical fish-tail structure.

183 More precisely:

184 - After 5 cm of shortening (Fig. 3c1), the lower sand layer is affected by a lower synthetic thrust
185 that penetrates the middle silicone layer. The middle sand layer is affected by a middle antithetic
186 thrust that penetrates into the upper silicone layer. The upper sand layer is affected by an upper
187 synthetic steeply dipping thrust with an incipient upper antithetic fault in its hanging wall. This
188 faulting pattern with opposing vergence is typical of a fish-tail structure. The synkinematic layers
189 show onlap geometry on the hanging wall of the upper thrust, and toplap geometry below the base
190 of the thrust in the footwall.

191 - After 7.5 cm of shortening (Fig. 3c2), the lower antithetic thrust penetrates deeply into the middle
192 silicone layer. The middle antithetic thrust has ceased growing and a new steeply dipping antithetic
193 thrust is formed cutting the upper sand layer and affecting the synkinematic layers. The upper
194 synthetic thrust ceases and a new upper antithetic thrust cuts the previous synthetic thrust and
195 synkinematic layers. The synkinematic layers show onlap geometry in the direction of the anticline
196 crest.

197 - After 10 cm of shortening (Fig. 3c3), the lower synthetic thrust penetrates deeply into the middle
198 silicone layer without anticline growth. The growth of the middle antithetic thrust continues until it
199 is cut by a new synthetic thrust. This thrust has variable dip, the lower part being nearly horizontal,
200 and the upper part steeply dipping (in yellow in Fig. 3c3). The vertical amplification of the

201 structures in the centre of the model is associated with a verticalization of the prekinematic layers.
202 The synkinematic layers show onlap geometry in the direction of the anticline crest.

203 *3.4. Shortening with synkinematic sedimentation, $R = 2$ (Fig. 3d)*

204 The main feature of this experiment is that all sand layers are affected by thrusts with opposing
205 vergence, thus developing a typical fish-tail structure. Finally, at the end of the shortening, the
206 deformation shows a double vergence.

207 More precisely:

208 - After 5 cm of shortening (Fig. 3d1), the lower sand layer is affected by a lower synthetic thrust
209 that penetrates into the middle silicone layer. The middle sand layer is affected by a middle
210 antithetic thrust that penetrates into the upper silicone layer. The upper sand layer is affected by a
211 major upper synthetic thrust and an incipient antithetic thrust. Although such a fault pattern with
212 opposing vergence is typical of a fish-tail structure, there is less folding and uplift in this case than
213 previously observed (Fig. 3c1). The synkinematic layers show a progressive decrease in the
214 thickness of the hanging wall in the direction of the upper synthetic thrust (in green in Fig. 3d1),
215 and a nearly constant thickness on its footwall. The thrusts near the piston in the middle and upper
216 sand layers are due to boundary effects at the beginning of the experiment (in grey in Fig. 3d).

217 - After 7.5 cm of shortening (Fig. 3d2), the deformation is similar to that observed for 5 cm of
218 shortening. The lower synthetic thrust shows deep penetration into the middle silicone layer. The
219 growth of the middle antithetic thrust continues and an incipient middle antithetic fault is formed.
220 The upper synthetic and antithetic thrusts are still active, associated with the development of a new
221 incipient antithetic thrust. The synkinematic layers show the same overall geometry as before.

222 - After 10 cm of shortening (Fig. 3d3), the lower synthetic thrust penetrates deeply into the middle
223 silicone layer, and the lower sand layer is also affected by an new antithetic thrust. The middle
224 antithetic thrust is cut by a middle synthetic thrust. The upper sand layer and the synkinematic
225 layers are affected by a synthetic and an antithetic thrust, as well as a new synthetic thrust. These
226 associated faults induce a double vergence in the deformation, and the synkinematic layers display a
227 relatively constant thickness.

228 *3.5. Time-evolution of structure uplift (Fig. 4)*

229 The time-evolution of the anticline crest uplift, which is associated with the thrusts, affects the
230 lower and upper sand layers in completely different ways depending on the R ratio. The maximum
231 uplift of the upper sand layer anticline is observed when the sedimentation rate is equal to the uplift
232 velocity ($R = 1$), and the minimum uplift is observed when there is no sedimentation ($R = 0$). On the
233 contrary, the maximum uplift of the lower sand layer structure is observed when there is no
234 sedimentation ($R = 0$) and minimum uplift occurs when the sedimentation rate is equal to or greater
235 than the velocity of uplift ($R = 2$ or 1). It is important to note that the amplitude of the uplift is
236 nearly the same (around 4 cm) for the lower and upper sand structure when there is no
237 sedimentation ($R = 0$). When the sedimentation rate is equal to the uplift velocity ($R = 1$), the
238 amplitude of the uplift in the upper sand layer is three times that of the lower sand layer (around 7.5
239 cm and 2.5 cm, respectively). Note that, when the sedimentation/uplift ratio is intermediate between
240 these two cases ($R = 1/2$, $E = 1/4$), the amplitude of the uplift is also intermediate. When the
241 sedimentation rate is double the uplift velocity ($R = 2$), the uplift of the lower sand layer structure
242 decreases to its minimum amplitude, while the uplift of the upper sand layer structure is lower than
243 for $R = 1$ and $R = 1/2$, with $E = 1/4$, as noted by Barrier et al. (2013).

244 4. Discussion

245 4.1. Influence of initial mechanical stratigraphy

246 The initial mechanical stratigraphy is characterized by the presence of interbedded silicone layers
247 and sand layers that allow decoupling between the sand layers.

248 Firstly, a typical flat lower thrust is developed because the lower sand layers penetrate into the
249 middle detachment level (see Fig. 5 for main features of experiments after 10 cm of shortening).
250 The geometry of the upper reverse fault is dependent on the sedimentation/uplift ratio (e.g. Pichot
251 and Nalpas, 2009; Barrier et al., 2013), and shows a maximum dip when $R = 1$ or 2 (Fig. 3a1, b1,
252 c1, d1 and 5, see $\alpha < \beta$). Secondly, two superposed thrusts with opposite vergence create a fish-tail
253 structure when the interbedded silicone layer acts as a decollement level (Figs. 3c1 and d1). These
254 fish-tail structures are created only when sedimentation occurs during deformation (for $R = 1$ and
255 2). In the experiment with low ratios of sedimentation and erosion with respect to uplift of the
256 structure ($R = 1/2$, $E = 1/4$), a fish-tail structure is only present between the lower and middle sand
257 layers (Fig. 3b). In the experiment without sedimentation, no fish-tail structures are created (Fig.
258 3a). Therefore, the presence of decollement levels is a necessary but insufficient condition to

259 produce such fish-tail structures. Thirdly, the presence of a decollement level allows the
260 deformation to propagate forward of the main upper structure (Figs. 3a2 and a3), provided there is
261 no sedimentation. Finally, we suggest it is necessary to have an initial mechanical stratigraphy with
262 several decollement levels to create specific features such as fish-tail structures and forward
263 propagation of the deformation. However, the presence of several decollement levels is insufficient
264 to explain the geometric evolution and variability of the structures.

265 *4.2. Influence of shortening*

266 Increasing shortening induces major deformation in the model, creating structures with a marked
267 uplift (Fig. 4), and an increase in the thrust throw. Firstly, during the increase in the amount of
268 shortening, two possible trends of development can be observed. When there is no sedimentation,
269 the model develops an overall asymmetric shape (Figs. 3a1 to a3). Alternatively, in the experiment
270 with sedimentation, the shape of the model evolves from asymmetric to doubly vergent (Figs. 3b3,
271 c1 to c3, and d1 to d3). Secondly, increased shortening enhances the penetration of thrusts into the
272 overlying silicone layer. Thirdly, although increased shortening allows the deformation to propagate
273 forward (Figs. 3a2 and a3), this can only take place in the absence of sedimentation. Finally, we
274 suggest that increased shortening is necessary to ensure an evolution in the overall shape of the
275 model, but is not sufficient to explain why this evolution is possible.

276 *4.3. Influence of synkinematic sedimentation*

277 The geometry of the structure is highly dependent on the sedimentation/uplift ratio (Figs. 3 and 5).
278 Without sedimentation, the geometry of structures is similar in the lower, middle and upper layers
279 insofar as they display the same synthetic vergence. Any increase in the shortening is
280 accommodated by a forward propagation of the deformation (Figs. 3a and 5a). By contrast, with
281 sedimentation, the geometry of the structures is different in the lower, middle and upper layers with
282 different vergence. Also there is no propagation of the deformation during shortening, and all the
283 structures are stacked above the VD (Figs. 3b, c, d and 5b, c).

284 With sedimentation, the geometry of the faults shows a fish-tail structure for the lower and middle
285 sand layers when $R = 1/2$ with ongoing erosion ($E = 1/4$), and for all layers when $R = 1$ and 2 (Figs.
286 3 and 5). This implies that more fish-tail structures are developed when the sedimentation rate is
287 higher. Such an effect may be related to an increase in normal stress induced by the synkinematic

288 layers, which increases the strength of the interbedded sand layers. In this way, the differential
289 strength between the sand and silicone layers increases, thereby making it easier for the sand layers
290 to penetrate the silicone layers.

291 During deformation, the overall shape of the model changes from asymmetric to doubly vergent,
292 with an increase in shortening that is only observed with synkinematic sedimentation. With an
293 increase in sedimentation with respect to uplift ($R = 1$ to 2), the model shows an increasingly
294 prominent doubly vergent shape.

295 In agreement with previous experimental studies (e.g. Tondji-Biyo, 1995; Nalpas et al., 1999;
296 Barrier et al., 2002; Nalpas et al., 2003; Pichot and Nalpas, 2009; Barrier et al., 2013), synkinematic
297 sedimentation strongly influences the uplift of compressive growth structures. When $R = 0$, the
298 effect of shortening in the lower and upper layers is the same, being associated with forward
299 propagation of the deformation without major uplift. The maximum uplift is found in the
300 experiment with $R = 1$ (Figs. 3, 4 and 5), but it is noteworthy that, when the uplift of the upper
301 structure increases, the lower structure undergoes less uplift (Fig. 4). When $R = 1$, the effect of
302 shortening in the lower and upper layers is different: the lower layer propagates horizontally, while
303 the upper layer grows vertically. The uplift of the lower structure is inhibited by the weight of the
304 sediments, which explains why there is minor uplift for $R = 2$, and major uplift for $R = 0$.

305 **5. Comparison with natural examples**

306 The structural style of the Bolivian Subandean foothills is characterized by elongated N-S trending
307 tight folds in the Chaco Basin (Figs. 6a and b). The geometry of the fold and thrust belt is mainly
308 controlled by lithology and the presence of three main potential decollement levels (Baby et al,
309 1989; Baby et al, 1992; Moretti et al., 1996; Giraudo and Limachi, 2001; Moretti et al., 2002). The
310 basal decollement level is located in the Kirusillas shales (Late Silurian). The middle decollement
311 levels are identified at Icla (Early Devonian) and Los Monos (Late Devonian), where potential
312 decollement is controlled by the clay content of the formations involved. The decollement levels
313 partly disconnect the deformation observed at the surface (Tertiary to Lower Carboniferous series)
314 from that occurring at depth (Devonian sandstones, Huamampampa, Fig. 6c). The upper
315 decollement level, which is the thinnest, is located in the Ipagueazu Formation, which is composed
316 of gypsum and shales (Triassic). Fluid overpressure in maturing source rocks may have an effect on
317 detachments and the propagation of deformation in compressive systems (Cobbold and Rodrigues,

318 2007; Cobbold et al., 2009), but we do not discuss this possibility here because we have only
319 analysed the geometry of isolated structures.

320 The Chaco Basin is a classical foreland basin in a retro arc position (Uba et al., 2005 and 2006).
321 Tertiary sedimentation is regarded as taking place in a foreland basin sequence during the Late
322 Oligocene to Early Miocene. The base of this sequence is represented by the unconformable fluvial
323 Petaca Formation (Late Oligocene to Early Miocene), which may be attributed to sedimentation in a
324 forebulge-backbulge depocentre. The overlying Yecua Formation (Middle to Late Miocene)
325 corresponds to the onset of active deformation and large-scale subsidence in response to thrust-belt
326 loading on a regional scale (distal foredeep). The overlying Tariquia Formation (Late Miocene) is
327 concomitant with the onset of deposition of Andean derived sediment in the medial-foredeep
328 depocentre. In our study area, eastward from the Incahuasi structure (Fig. 6b), these formations may
329 be considered as of relatively constant thickness and are thus pre-tectonic. In the western part of our
330 study area, westward from the Incahuasi structure (Fig. 6b), these formations are of variable
331 thickness and may be considered as syn-tectonic.

332 The Guandacay Formation (Late Miocene to Early Pliocene) and Emborozu Formation (Late
333 Pliocene to Pleistocene) are coeval with the propagation of the deformation front in the Subandean
334 Zone and thus represent true syntectonic deposits associated with the emplacement of the folds and
335 thrusts in our studied area (Incahuasi structure). Their thickness can vary between 1000 - 3500 m.
336 The age of the Guandacay Formation corresponds to the peak of shortening calculated by Moretti et
337 al. (1996).

338 As hydrocarbon exploration in Bolivia targets a deep-seated reservoir below the main upper
339 decollement (Devonian Los Monos Formation), some of these N-S trending tight folds have been
340 drilled and some seismic data exists. The quality of seismic data in the Subandean Zone is poor and
341 this hinders clear imaging of the deep-seated structures. Therefore, it is difficult to interpret the
342 seismic data, which often give rise to misleading interpretations. Among the folds in the area, the
343 Incahuasi anticline shows some interesting features. Three exploration wells drilled on the anticline
344 axis confirm that the top of the Huamampampa Formation is offset by at least 1 km to the east with
345 respect to the surface anticline axial plane (Fig. 7) as evidenced by sampling and dipmeter data
346 acquired during drilling. The surface Incahuasi structure is overturned towards the west and shows a
347 vergence contrary to that of most other folds in the Subandean Zone (Fig. 6). The main backthrust
348 that accommodates this overfolding is rooted in the basal shale of the Los Monos Formation, close

349 to the interface with the Huamampampa quartzites. The dipmeter data in wells confirm the fact that
350 the deep-seated thrust system affecting the Huamampampa Formation also faces towards the west
351 (hinterland). Geological cross-sections constrained by field and several wells data confirm that the
352 Incahuasi thrust, facing towards the east, has been passively rotated by the emplacement of the
353 backthrust (Figs. 6 and 7), which postdates the Incahuasi thrust, in the same way as reproduced by
354 analogue modelling (Figs. 3b).

355 A comparison between the Incahuasi subsurface data and the analogue experiments (inverted cross-
356 section of the model of figure 3b3) allows us to propose an interpretation of the Incahuasi structure
357 in a cross-section showing the evolution of the thrust in time and space (Fig. 7). The overall
358 evolution corresponds to an inversion of the vergence of the thrust. The first fault propagation fold
359 is cut and displaced passively along with the hanging wall of the newly formed thrust fault.
360 Therefore, the change in the vergence of the Incahuasi fold may be explained by the influence of
361 sedimentation rate. Figure 7 compares the subsurface data, their interpretation and the interpreted
362 cross-section of a model, showing the positive contribution of analogue modelling to an improved
363 interpretation of the seismic lines.

364 A comparison can also be made between the experimental results and subsurface data for the whole
365 cross-section of the Subandean system (Fig. 6b). We propose that, in the eastern part, the structures
366 of Camiri, Carohuaycho Los Huesos, Caipipendi and Charagua are characterized by major
367 asymmetric geometries and propagation of deformation in front of the thrust, which is characteristic
368 of the experiment with low sedimentation rate (Figs. 3a and 5a). The central zone corresponding to
369 the Incahuasi structure shows a drastic change in vergence direction, which is comparable to the
370 experiment with a medium rate of sedimentation (Figs. 3b and 5b). The western structures of
371 Ilinchunpa and Inau are characterized by a double vergence and vertical propagation of the
372 deformation, corresponding to the experiment with high sedimentation rate (Figs. 3c3, d3; and 5c).
373 Thus, this lateral variation in the structures (see also Baby et al., 1992; Moretti et al., 1996; Giraudo
374 and Limachi, 2001; Moretti et al., 2002) is consistent with an increase in shortening from east to
375 west and a decrease in rate of sedimentation from the hinterland toward the foreland.

376 **6. Conclusions**

377 The experimental results presented here suggest that:

378 a - The initial mechanical stratigraphy and the presence of several decollement levels are necessary
379 conditions for the creation of specific features related to decoupling between sand layers, such as
380 fish-tail structures and the propagation of deformation. However, these conditions alone cannot
381 explain the evolution and variability in the geometries of the structures.

382 b - The final geometry of the structure seems to be highly dependent on the sedimentation/uplift
383 ratio, R . When $R = 0$ (no sedimentation), the deformation propagates forward with an overall
384 asymmetric shape. When $R = 1/2$ or 1 (low sedimentation rate), the deformation increases vertically
385 with steeply dipping faults, and the vergence of the structure changes with the development of a
386 thrust with opposite vergence. When $R = 2$ (high sedimentation rate), the deformation creates a
387 pattern of doubly vergent structures at the surface and at depth, with the development of a conjugate
388 structure and associated uplift.

389 c - The expression of deformation in the brittle layers below the upper decollement levels is
390 different compared with layers above the upper decollement levels, and depends on decoupling and
391 sedimentation rate. With low mass transfer (low sedimentation rate), the lower and upper brittle
392 layers are deformed in the same way with the same amount of uplift. On the other hand, with high
393 mass transfer (high sedimentation rate), the lower brittle layers show much less uplift than the upper
394 brittle layers.

395 d - Application of the analogue modelling results to the Subandean compressive system suggests
396 that the west to east evolution of the structures in the thrust and fold belt (from doubly vergent with
397 several faults and large uplift to asymmetric with a single major fault) is related to the variation in
398 the amount of shortening and sedimentation rate.

399 e - Seismic lines have low resolution in compressive systems with intense deformation and steeply
400 dipping layers. Therefore, in such a context, analogue modelling can be a useful tool for exploring
401 the geometric possibilities in relation to the evolution of structures, allowing us to improve the
402 interpretation of seismic lines.

403

404 **Acknowledgements:**

405 We acknowledge Total for financial support. Special thanks are due to J.-J. Kermarrec for his

406 valuable technical assistance and availability. We thank Sara Mullin, Noelle Odling and Mike
407 Carpenter for their editing of the English style. Finally, we are grateful to P. Cobbold and C. Gomes
408 for their detailed review, constructive comments and suggestions that helped us improve an early
409 version of the manuscript.

410

411 **References**

- 412 Allemand, P., Brun, J.-P., Davy, P., Van Den Driessche, J., 1989. Symétrie et asymétrie des rifts et
413 mécanismes d'amincissement de la lithosphère. *Bulletin de la Société Géologique de France* 3, 445-451.
- 414 Baby, P., Hérail, G., Lopez, J.M., Lopez, O., Oller, J., Pareja, J., Sempere, T., Tufiño, D., 1989. Structure de
415 la Zone Subandine de Bolivie: influence de la géométrie des séries sédimentaires antéorogéniques sur la
416 propagation des chevauchements. *Comptes Rendus de l'Académie des Sciences*, 309, 1717-1722.
- 417 Baby, P., Hérail, G., Salinas, R., Sempere, T. 1992. Geometric and kinematic evolution of passive roof
418 duplexes deduced from cross section balancing: example from the foreland thrust system of the
419 southern Bolivian Subandean Zone. *Tectonics*, 11, 523-536.
- 420 Baby, P., Colletta, B., Zubieta, D., 1995. Etude géométrique et expérimentale d'un bassin transporté:
421 exemple du synclinorium de l'Alto Beni (Andes centrales). *Bulletin de la Société Géologique de France*,
422 166, 797-811.
- 423 Balé, P., 1986. Tectonique cadomienne en Bretagne nord. Interaction décrochement chevauchement :
424 champs de déformation et modélisations expérimentales. Ph.D. thesis, Université de Rennes 1.
- 425 Ballard, J.F., Brun, J.P., Van Den Driessche, J., Allemand, P., 1987. Propagation des chevauchements au-
426 dessus des zones de décollement : Modèles expérimentaux. *Comptes Rendus de l'Académie des Science*
427 *de Paris, Série IIA* 305, 1249-1253.
- 428 Ballard, J.F., 1989. Approche géologique et mécanique des décollements dans la croûte supérieure. Ph.D.
429 thesis, Université de Rennes 1.
- 430 Barrier, L., Nalpas, T., Gapais, D., Proust, J.-N., Casas, A., Bourquin, S., 2002. Influence of syntectonic
431 sedimentation on thrusts geometry. Field examples from the Iberian Chain (Spain) and analogue
432 modeling. *Sedimentary Geology* 146, 91-104.

- 433 Barrier, L., Nalpas, T., Gapais, D., Proust, J.-N., 2013. Impact of synkinematic sedimentation on the
434 geometry and dynamics of compressive growth structures: Insights from analogue modelling.
435 *Tectonophysics* 608, 737-752.
- 436 Boyer, S.E., Elliott, D., 1982. Thrust systems. *American Association of Petroleum Geologists Bulletin* 66,
437 1196-1230.
- 438 Casas, A.M., Gapais, D., Nalpas, T., Besnard, K. Roman Berdiel, T., 2001. Analogue models of
439 transpressive systems. *Journal of Structural Geology* 23, 733-743.
- 440 Cobbold, P.R., Davy, P., Gapais, D., Rossello, E.A., Sadybakasov, E., Thomas, J.C., Tondji Biyo, J.J., de
441 Urreiztieta, M., 1993. Sedimentary basins and crustal thickening. *Sedimentary Geology*, 86, 77-89.
- 442 Cobbold, P.R., Castro, L., 1999. Fluid pressure and effective stress in sandbox models. *Tectonophysics* 301,
443 1-19.
- 444 Cobbold, P.R., Durand, S., Mourgues, R., 2001. Sandbox modelling of thrust wedges with fluid-assisted
445 detachments. *Tectonophysics* 334, 245-258.
- 446 Cobbold, P.R., Rodrigues, N., 2007. Seepage forces, important factors in the formation of horizontal
447 hydraulic fractures and bedding-parallel fibrous veins (“beef” and “cone-in-cone”). *Geofluids* 7, 313-
448 332.
- 449 Cobbold, P.R., Clarke, B.J., Løseth, H., 2009. Structural consequences of fluid overpressure and seepage
450 forces in the outer thrust belt of the Niger Delta. *Petroleum Geoscience* 15, 3-15.
- 451 Cohen H.A., McClay K.R., 1996. Sedimentation and shale tectonics of the northwestern Niger Delta front.
452 *Marine and Petroleum Geology* 13, 313-328.
- 453 Couzens-Schultz, B., Vendeville, B. Wiltschko, D., 2003. Duplex style and triangle zone formation: insights
454 from physical modeling. *Journal of Structural Geology* 25, 1623-1644.
- 455 Davy, P., Cobbold, P. R., 1991. Experiments on shortening of a 4-layer model of continental lithosphere.
456 *Tectonophysics* 188, 1-25.
- 457 Dunn, J. F., Hartshorn, K. G., Hartshorn, P. W., 1995. Structural styles and hydro- carbon potential of the
458 sub-Andean thrust belt of southern Bolivia. In: Tankard, A. J., Suárez Soruco, R., Welsink, H. J. (Eds.),
459 *Petroleum basins of South America: AAPG Memoir* 62, 523-543.

- 460 Faugère, E. Brun, J.-P., 1984. Modélisation expérimentale de la distension continentale. *Comptes-Rendus de*
461 *l'Académie des Sciences* 299, 365-370.
- 462 Gestain, V., Nalpas, T., Rouby, D., Barrier, L., 2004. Rôle des niveaux incompétents syncinématiques sur
463 l'évolution des structures chevauchantes. *Bulletin de la Société Géologique de France* 175, 351-359.
- 464 Giraudo R., Limachi R., 2001. Pre-Silurian control in the genesis of the central and southern Bolivian fold
465 belt. *Journal of South American Earth Science* 14, 665-680.
- 466 Horton, B.K., 1999. Erosional control on the geometry and kinematics of thrust belt development in the
467 central Andes. *Tectonics* 18, 1292-1304.
- 468 Krantz, R. W., 1991. Measurements of friction coefficients and cohesion for faulting and fault reactivation in
469 laboratory models using sand and sand mixtures. *Tectonophysics* 188, 203-207.
- 470 Labaume, P., Moretti, I., 2001. Diagenesis-dependence of cataclastic thrust fault zone sealing in sandstones.
471 Example from the Bolivian Sub-Andean Zone. *Journal of Structural Geology* 21, 1659-1675.
- 472 Leturmy, P., Mugnier, J.L., Vinour, P., Baby, P., Colletta, B., Chabron, E., 2000. Piggyback basin
473 development above a thin-skinned thrust belt with two detachment levels as a function of interactions
474 between tectonic and superficial mass transfer: the case of the Subandean Zone
475 (Bolivia). *Tectonophysics* 320, 45-67.
- 476 Malavieille, J. 1984. Modélisation expérimentale des chevauchements imbriqués: application aux chaînes de
477 montagnes, *Bulletin de la Société Géologique de France* 26, 129-138.
- 478 Massoli, D., Koyi, H. A., Barchi, M. R., 2006. Structural evolution of a fold and thrust belt generated by
479 multiple décollements: analogue models and natural examples from the Northern Apennines (Italy).
480 *Journal of Structural Geology* 28, 185-199.
- 481 Moretti, I., Baby, P., Mendez, E., Zubieta, D., 1996. Hydrocarbon generation in relation to thrusting in the
482 Sub Andean zone from 18 to 22 degrees S, Bolivia. *Petroleum Geoscience* 2, 17-28.
- 483 Moretti, I., Labaume, P., Sheppard, S.M.F., Boulègue, J., 2002. Compartmentalisation of fluid migration
484 pathways in the sub-Andean Zone, Bolivia. *Tectonophysics* 348, 5-24.
- 485 Mourgues, R., Cobbold, P.R., 2003. Some tectonic consequences of fluid overpressures and seepage forces
486 as demonstrated by sandbox modelling. *Tectonophysics* 376, 75-97.

- 487 Nalpas, T., Györfi, I., Guillocheau, F., Lafont, F., Homewood, P., 1999. Influence de la charge sédimentaire
488 sur le développement d'anticlinaux synsédimentaires. Modélisation analogique et exemples de terrain
489 (Bordure sud du bassin de Jaca). *Bulletin de la Société Géologique de France* 170, 733-740.
- 490 Nalpas, T., Gapais, D., Verges, J., Barrier, L., Gestain, G., Leroux, G., Rouby, D., Kermarrec, J.J., 2003.
491 Effects of rate and nature of synkinematic sedimentation on the growth of compressive structures
492 constrained by analogue models and field examples. *Geological Society of London Special Publication*
493 208, 307-319.
- 494 Pichot, T., Nalpas, T., 2009. Influence of synkinematic sedimentation in a thrust system with two
495 decollement levels; analogue modeling. *Tectonophysics* 473, 466-475.
- 496 Posamentier, H.W., Jervey, M.T., Vail, P.R., 1988. Eustatic controls on clastic deposition I - conceptual
497 framework. In: Wilgus, C.K., Hastings, B.S., Kendall, C.G.St.C., Posamentier, H.W., Ross, C.A., Van
498 Wagoner, J.C. (Eds.), *Sea Level Changes - An Integrated Approach*. Special Publication, vol. 42.
499 Society of Economic Paleontologists and Mineralogists (SEPM), 110-124.
- 500 Posamentier, H.W., Vail, P.R., 1988. Eustatic controls on clastic deposition II - sequence and systems tract
501 models. In: Wilgus, C.K., Hastings, B.S., Posamentier, H.W., Van Wagoner, J., Ross, C.A., Kendall,
502 C.G.St.C. (Eds.), *Sea-level Changes - An Integrated Approach*, vol. 42. SEPM Publication, 125-154.
- 503 Richard, P., Mocquet, B., Cobbold, P.R., 1991. Experiments on simultaneous faulting and folding above a
504 basement wrench fault. *Tectonophysics* 188, 133-141.
- 505 Seppehr, M., Coscrove, J. W. Moieni, M. 2006. The impact of cover rock rheology on the style of folding in
506 the Zagros fold-thrust belt. *Tectonophysics* 427, 265-81.
- 507 Smit, J.H.W., Brun, J.-P., Sokoutis, D., 2003. Deformation of brittle-ductile thrust wedges in experiments
508 and nature. *Journal of Geophysical Research* 108, B10, 2480, doi: 10.1029/2002JB002190.
- 509 Storti, F., McClay, K., 1995. Influence of syntectonic sedimentation on thrust wedges in analogue models.
510 *Geology* 23, 999-1002.
- 511 Tondji Biyo, J.J., 1995. Chevauchements et bassins compressifs. Influence de l'érosion et de la
512 sédimentation. *Mémoires de Géosciences Rennes*.
- 513 Uba, C.E., Heubeck, C., Hulka, C., 2005. Facies analysis and basin architecture of the Neogene Subandean
514 synorogenic wedge, southern Bolivia. *Sedimentary Geology* 180, 91-123. doi:
515 10.1016/j.sedgeo.2005.06.013.

- 516 Uba, C.E., Heubeck, C., Hulka, C., 2006,.Evolution of the late Cenozoic Chaco foreland basin, southern
517 Bolivia. Basin Research 18, 145-170, doi: 10.1111/j.1365-2117.2006.00291.x.
- 518 Verges, J., Goodarzi, M. G. H., Emami, H., Karpuz, R., Efstathiou, J., Gillespie, P., 2011. Multiple
519 detachment folding in Pusht-e Kuh arc, Zagros: Role of mechanical stratigraphy. In: McClay, K., Shaw,
520 J., Suppe, J. (Eds.), Thrust fault-related folding: AAPG Memoir 94, 69-94.
- 521 Weijermars, R., Jackson, M.P.A., Vendeville, B., 1993. Rheological and tectonic modeling of salt provinces.
522 Tectonophysics 217, 143-174.
- 523 Wu, J.E., McClay, K.R., 2011. Two-dimensional analog modelling of fold and thrust belts: Dynamic
524 interactions with syncontractional sedimentation and erosion. In: K. McClay, J. Shaw, J. Suppe, (Eds.),
525 Thrust fault-related folding: AAPG Memoir 94, 301-333.
- 526 YPFB-SERGEOMIN, 1996. Mapa geológico de Bolivia 1:1 000 000.
- 527 Zanella, A., Cobbold, P.R., Le Carlier de Veslud, C., 2014. Physical modelling of chemical compaction,
528 overpressure development, hydraulic fracturing and thrust detachments in organic-rich source rock
529 Original Research. Marine and Petroleum Geology, Article In Press.

530

531 **Figure and Table captions**

532 *Figure 1: (a) Experimental apparatus and (b) sketch of the homogeneous and local synkinematic*
533 *sedimentation. R is the ratio between the sedimentation rate, V_s , and the velocity of structure uplift,*
534 *V_u ($R = V_s/V_u$, see Barrier et al., 2002). E is the ratio between the erosion rate, V_e , and the*
535 *velocity of structure uplift, V_u ($E = V_e/V_u$).*

536 *Figure 2: Cross-section showing the terminology used in the description of the experiments.*

537 *Figure 3: Cross-sections of experiments for 5, 7.5, 10 cm of shortening. a1 to a3: for $R = 0$; b1 to*
538 *b3; for $R = 1/2$ and $E = 1/4$; c1 to c3: for $R = 1$; d1 to d3: for $R = 2$. The colour coding used is*
539 *green for a fault active only at the beginning of deformation, red for a fault active throughout*
540 *deformation and yellow for a fault active at the end of deformation. "Bode" and "Repa" denote*
541 *different experiments.*

542 *Figure 4: Diagram showing time-evolution of uplift of the upper and lower structures during*
543 *compression.*

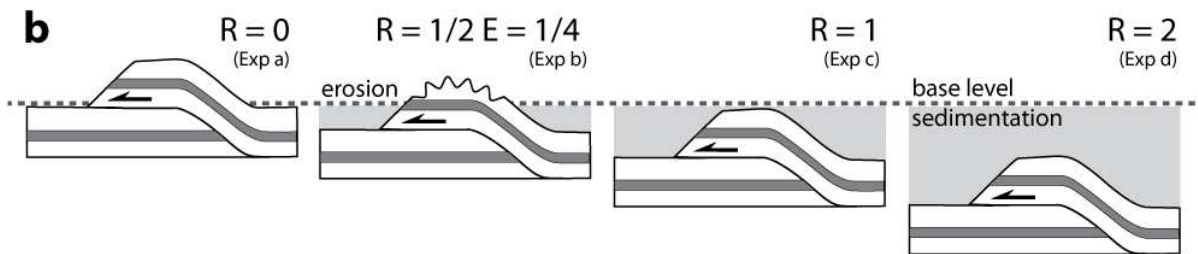
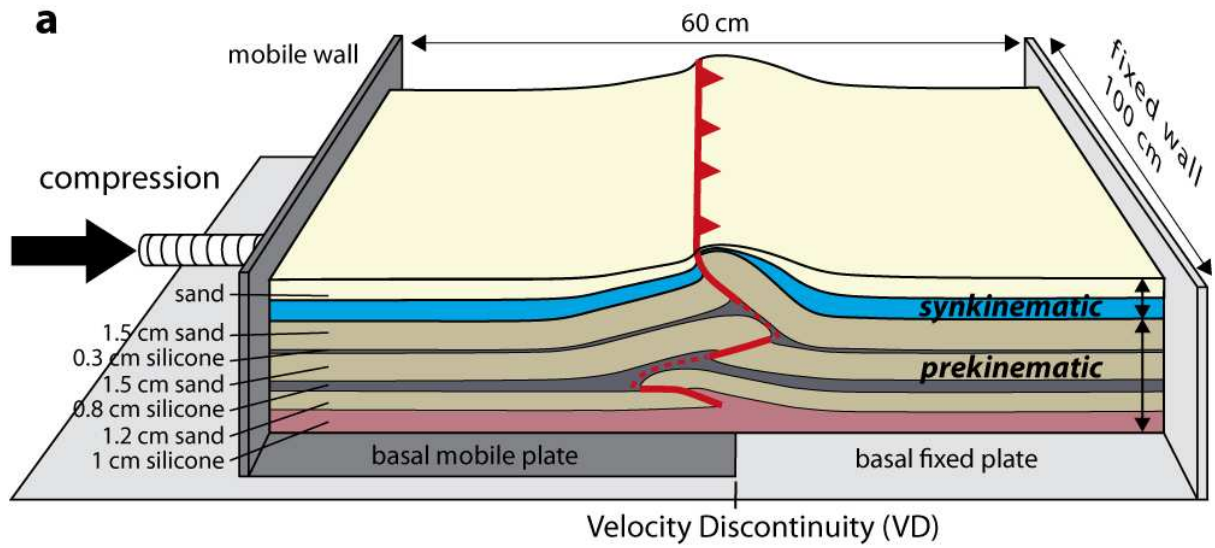
544 *Figure 5: Schematic cross-section of experiments after 10 cm of shortening showing the main*
545 *features of the structures.*

546 *Figure 6: (a) Geological map of Bolivia showing location of the interpreted seismic line (YPFB-*
547 *SERGEOMIN, 1996). (b) Cross-section of the Subandean fold and thrust belts across the Incahuasi*
548 *structure (using surface and subsurface data), the names correspond to the main structures. (c)*
549 *Stratigraphic column of the Bolivian Subandean Zone (Moretti et al., 2002), interpreted in terms of*
550 *mechanical stratigraphy, compared with structures obtained in the analogue experiments.*

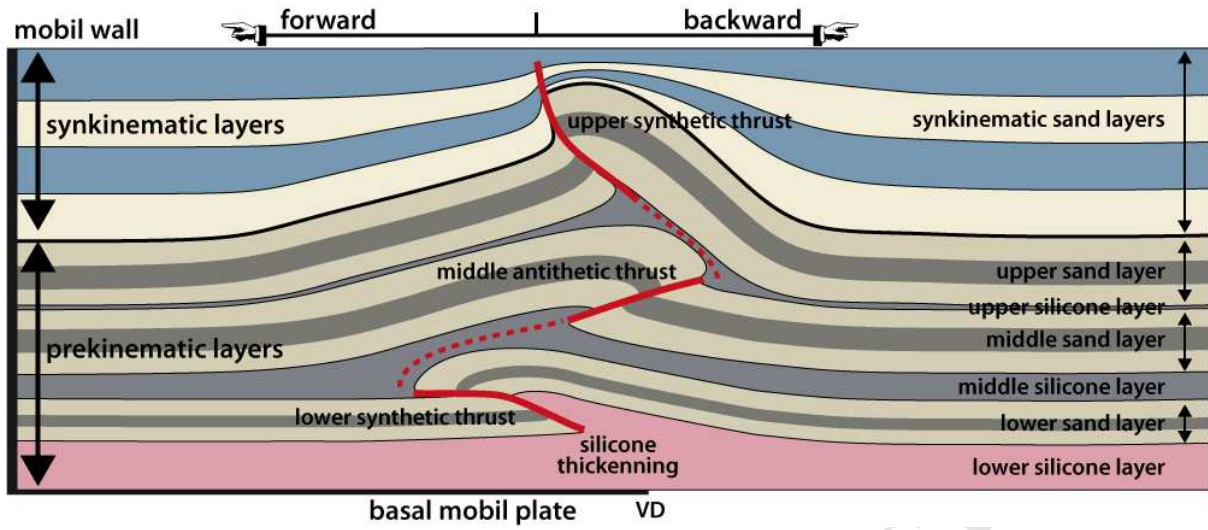
551 *Figure 7: (a) Subsurface data (seismic line and well) for the Incahuasi structure. (b) Interpretation*
552 *of the Incahuasi structure (c) Inverted cross-section of experiment b after 10 cm of shortening (see*
553 *figure 3b3).*

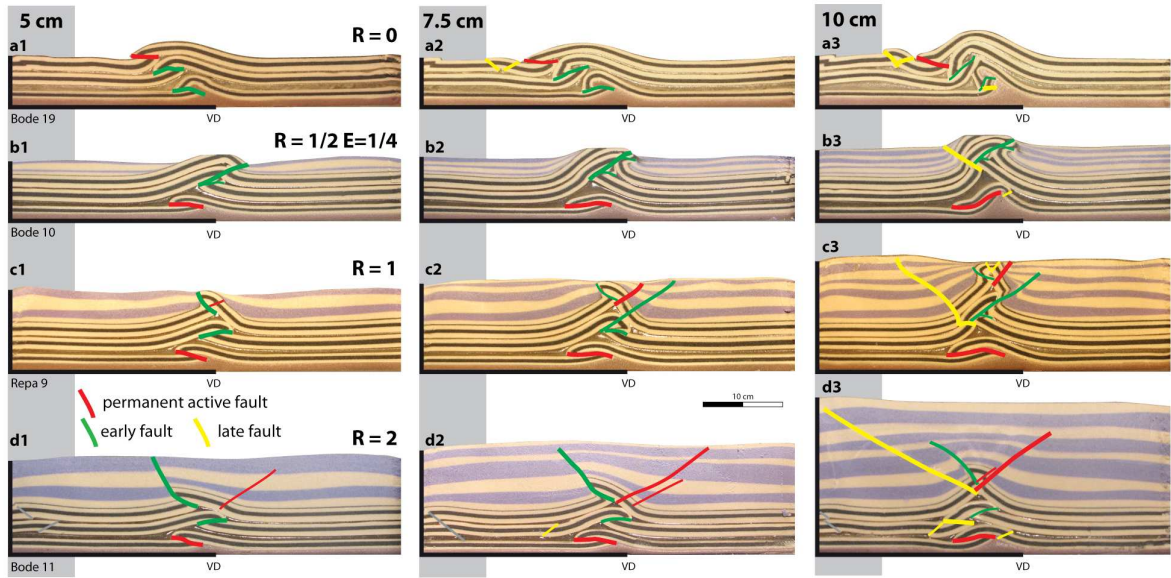
554 *Table 1: Scaling of parameters between nature and models. L , g , ρ , μ , V , t , and σ represent the*
555 *length, acceleration due to gravity, density, viscosity, shortening rate, time and stress, respectively.*

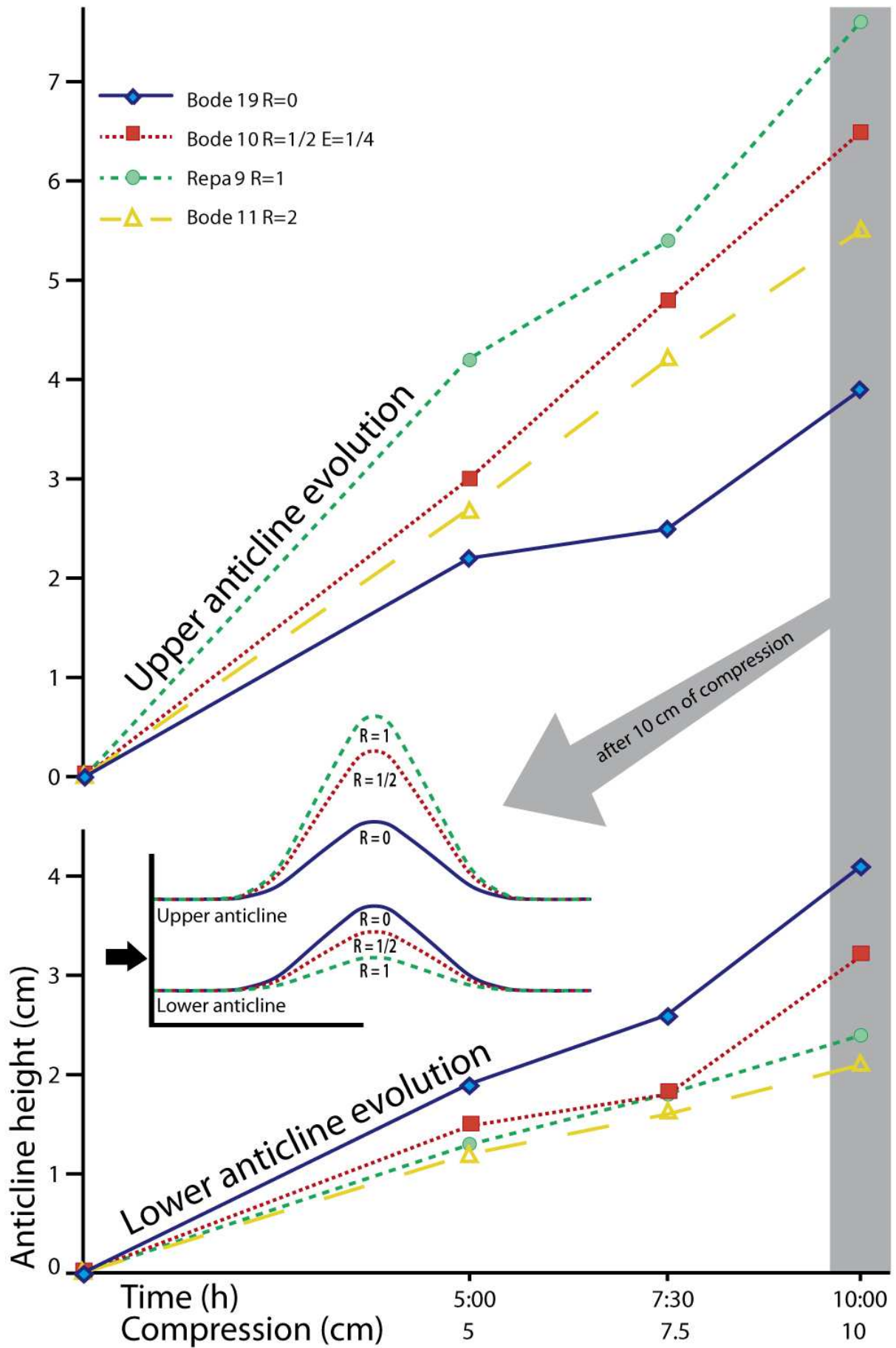
	L (m)	g (m/s ²)	ρ (kg/m ³)	μ (Pa·s)	V (m/s)	t (s)	σ (Pa)
Nature	1000 (1 km)	9.81	2300	2×10^{17}	3.2×10^{-10} (±1cm/year)	3.1×10^{12} (1 Ma)	2.2×10^7
Model	0.01 (1 cm)	9.81	1400	1.4×10^4	2.7×10^{-06} (1 cm/h)	3.6×10^3 (10 h)	1.3×10^2
Model/nature ratio	10^{-05}	1	0.6	7×10^{-15}	8.7×10^{03}	1.1×10^{-09}	6.1×10^6

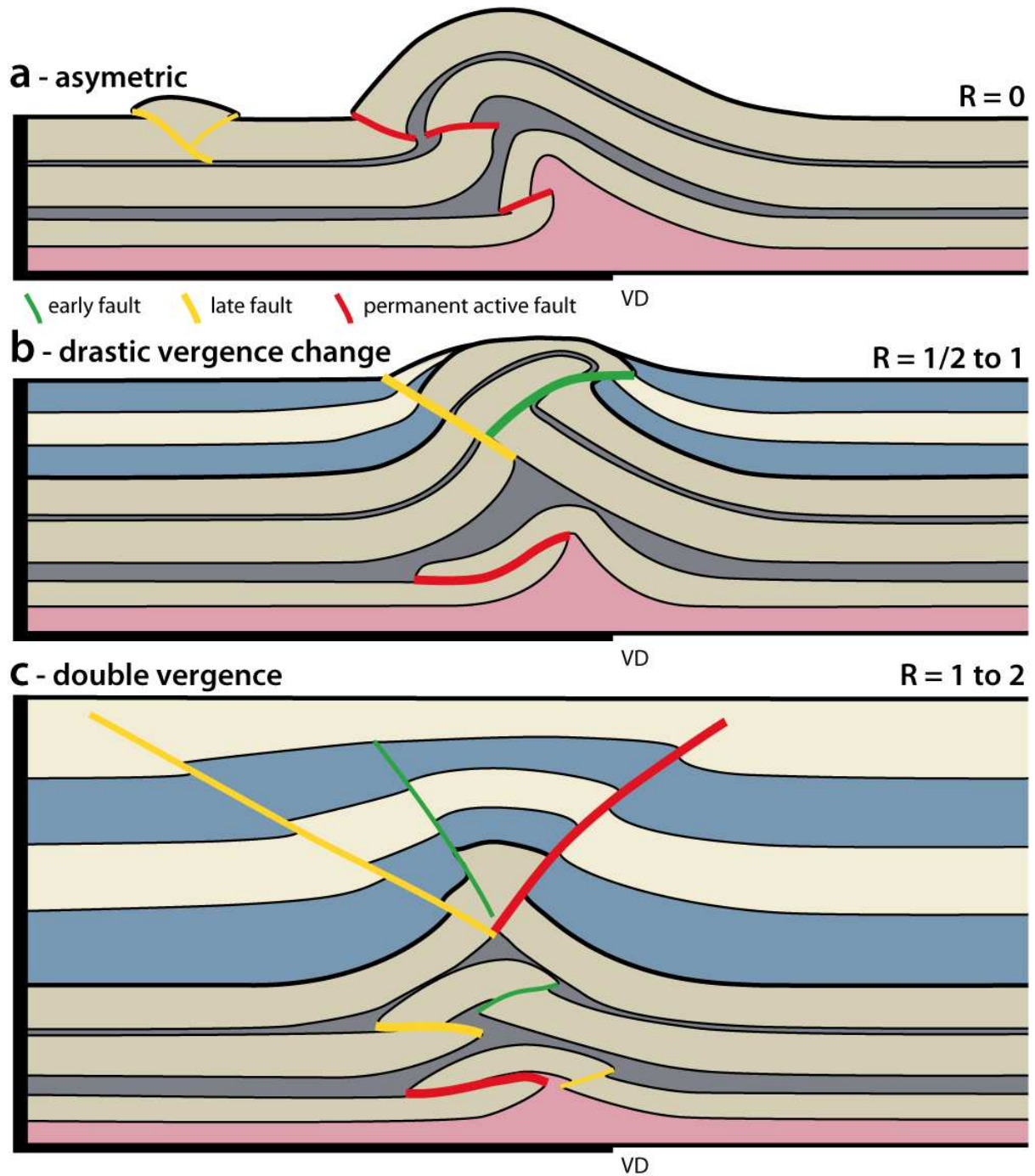


ACCEPTED MANUSCRIPT

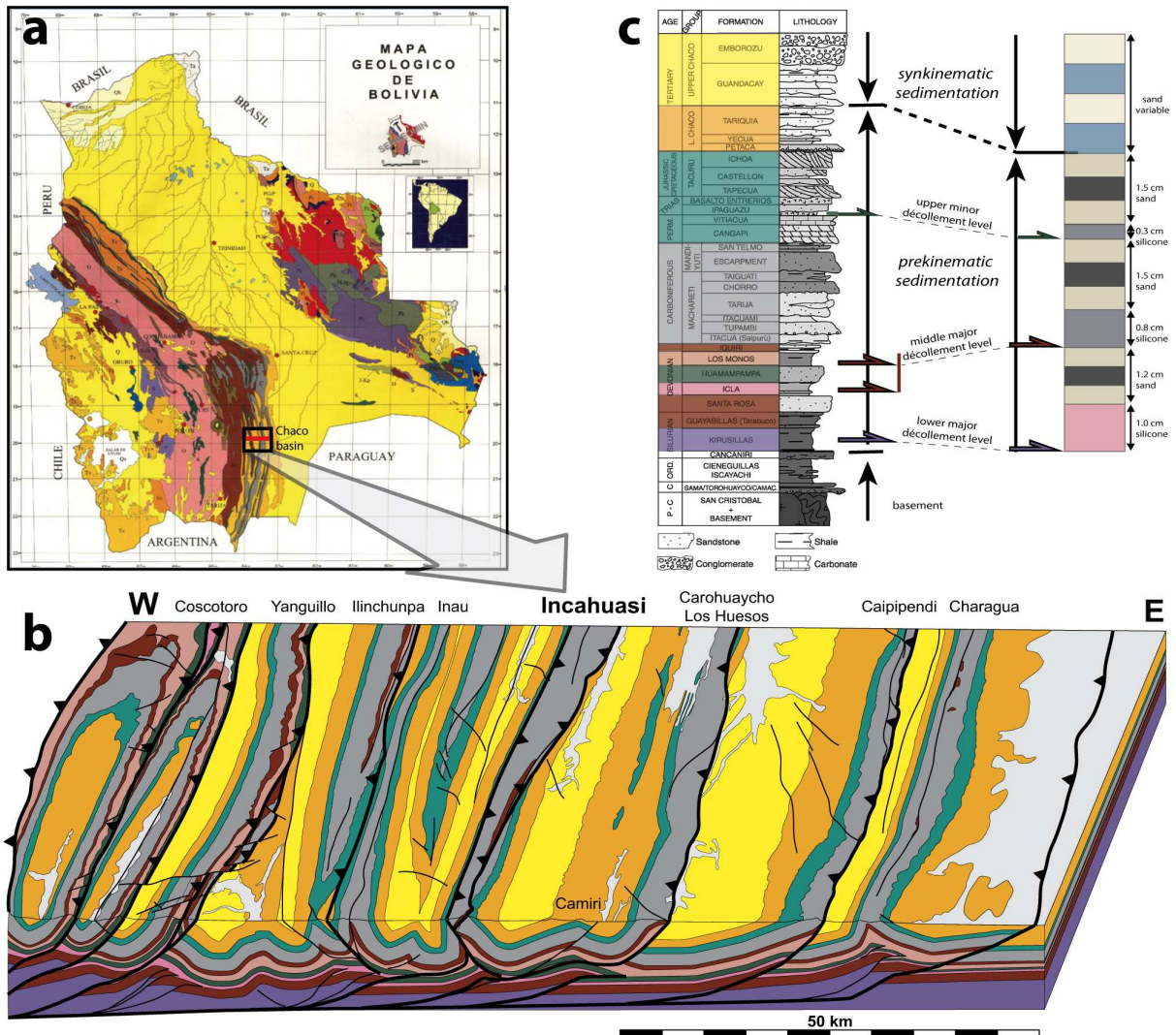




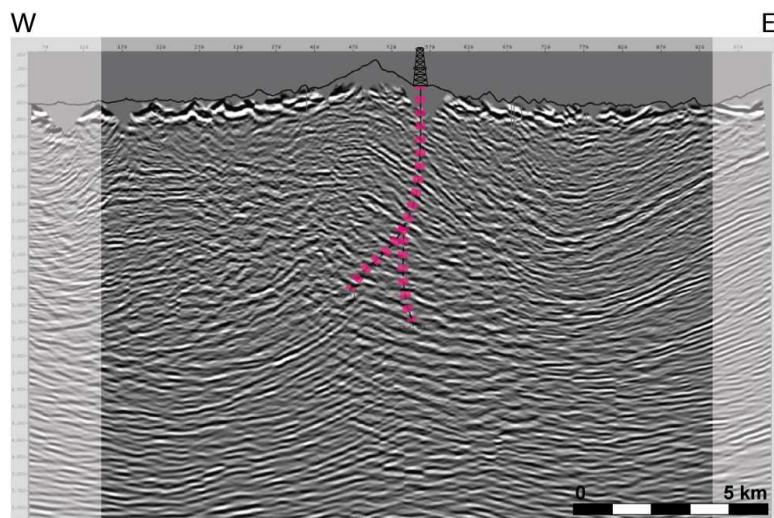




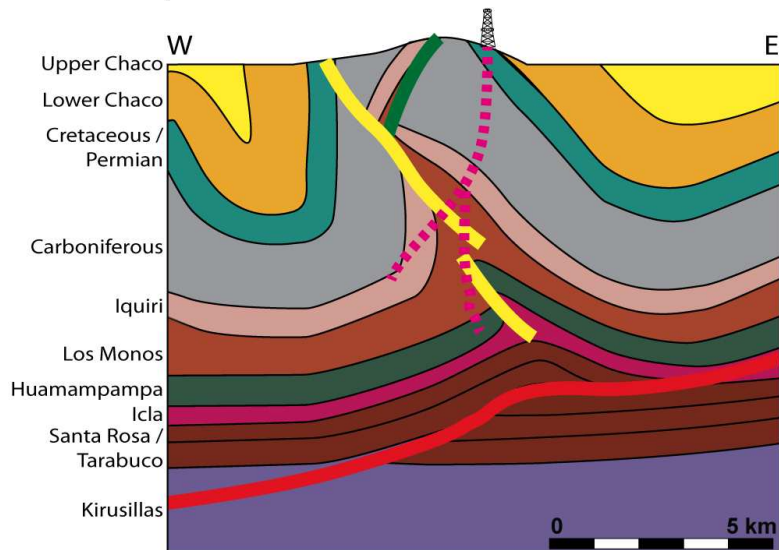
AC



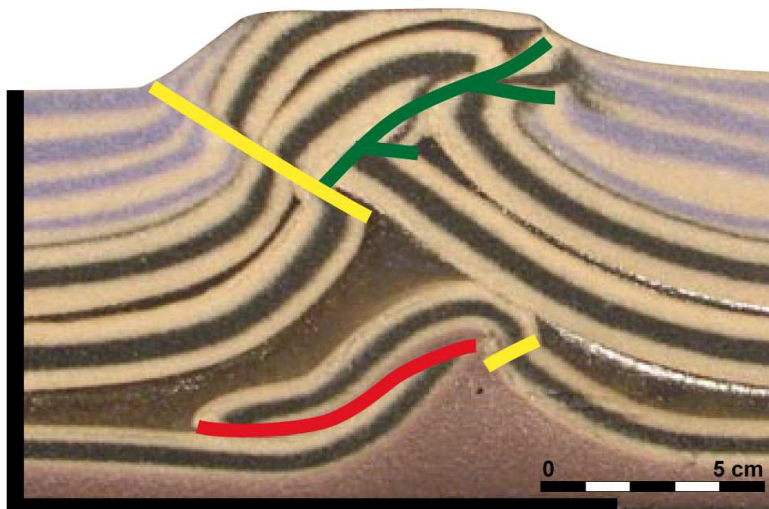
a - Subsurface data



b - Interpretation of Incahuasi structure



c - Cross-section of experiment



\ permanent active fault
 \ early fault
 \ late fault

HIGHLIGHTS

- With décollement levels, models of compressive system show fish-tail structure
- Synkinematic sedimentation favour vertical uplift and double vergence in thrust structure
- Models allow to better interpret seismic lines in compressive systems
- The evolution of Subandean structures is related to shortening and mass transfer